Measuring the viscosity of air with soapy water, a smartphone, a funnel and a hose: An experiment for undergraduate physics students

Alexandre Delvert, Pascal Panizza, Laurent Courbin

Measuring the viscosity of air with soapy water, a smartphone, a funnel and a hose: An experiment for undergraduate physics students

Alexandre Delvert,[1] Pascal Panizza,[1,2,*] and Laurent Courbin[1,†]

[1] *Univ Rennes, CNRS, IPR (Institut de Physique de Rennes) - UMR 6251, F-35000 Rennes, France*
[2] *Laboratoire Sciences et Ingénierie de la Matière Molle, ESPCI Paris, PSL University, Sorbonne Université, CNRS UMR 7615, F-75005 Paris, France*

(Received; Accepted)

We investigate the spontaneous motion of a soap film in a conical geometry connected to a long tube and show how it can be used to measure the dynamic viscosity of air. In contrast to other techniques that are complicated to implement and require expensive and sophisticated equipment, this measurement method relies only on soapy water and three everyday life objects: a smartphone, a funnel and a hose. More precisely, to determine the viscosity of air, we use a smartphone to record the spontaneous motion of a soap film placed in a funnel when the motion of the film is quasistatic and the flow of air escaping the geometry is viscously dominated. This simple experiment should be of value to undergraduate physics students in learning about effects of both fluid viscosity and surface tension (another fluid property which they could also measure with a smartphone)[1], and the usefulness of reasonable approximations in physics.

I. INTRODUCTION

Two of the main parameters associated with fluid dynamics are a fluid's viscosity, which characterizes its resistance to flow, and surface tension, which is the energy needed to increase the surface area of a fluid interface by one unit.[2] We regularly see effects of surface tension in our everyday life, e.g., whenever we blow soap bubbles.[2,3] Because of surface tension, the liquid film forming the bubble minimizes its surface area to seek a spherical shape. Like surface tension, a fluid's viscosity originates from molecular effects and its consequences can be seen at a macroscopic level: when shaking a jar of honey, physics students at any level guess correctly that it is a highly viscous liquid compared to water. Sophisticated and expensive equipment for tensiometry and rheology can be used to fully characterize these two fluid parameters. It is interesting to note, however, that the literature documents simple and inexpensive ways that students can measure the air-liquid surface tension or the viscosity of a liquid. Therefore, these methods could be useful in introductory-level physics laboratories.[1,4] For instance, liquid-air surface tension can be determined using the camera of a smartphone and a ruler to characterize the shape of a pendant drop.[1] Also, liquid viscosity can be measured using a weight-controlled capillary viscometer,[4] measurements being based in this case on the simple determination of the rate at which liquid drains from a tank through a capillary tube.

In sharp contrast with measuring the viscosity of liquids, measuring that of gases is not an easy task. For example, the dynamic viscosity of air is $\eta_a = 18.1$ μPa s at 20 °C, roughly 50 times smaller than that of water, and too small to be measured with standard rheometry because of the mechanical friction inherent in this type of equipment. Instead, one can use a custom-built viscometer that can be complicated to implement, such as a friction-free electromagnetic spinning system based on the diamagnetic levitation of graphite.[5] As an alternative to these complicated experiments, in this paper, we present a device that allows students to measure the viscosity of air at low cost with simple equipment : soapy water, a funnel, some tubing and a smartphone camera.

The experiment consists of recording and analyzing the spontaneous motion of a soap bubble film in a funnel that has a long and narrow neck. Such a film moves on the sloping sides of a funnel from its wide opening toward its narrow end, and, as it moves, it pushes air out through the neck of the funnel. The outward motion of air is resisted by its dynamic viscosity. By timing this motion, we learn how fast the air is pushed out, and knowing the geometric parameters of the funnel and air-liquid surface tension, the viscosity of air can be found. This experiment resembles a recent study in which we discuss different scenarios of shrinking surface soap bubbles sitting on a thin solid with an orifice located under the apex of the bubble.[6] In one of these scenarios, also driven by Laplace pressure,[7] a bubble remains hemispherical as it shrinks so that the contact angle made by the bubble with the solid remains close to $\pi/2$ as the base of the bubble moves towards the orifice. The differences between these experiments are that the soap bubble in this experiment moves on an incline instead of a flat surface and the air flow satisfies Poiseuille's law rather than Bernoulli's principle. It is worthwhile noting that the described experiment can also be seen as a simple self-propelling system with which students would observe soap films moving against gravity. Other studies found in the literature discuss methods that are often costly and difficult to implement and rely on suitable surface chemistry or controlled surface topography to produce the self-propulsion of fluids on solids.[8–10] For example, the use of controlled gradients of surface chemistry of a solid can make a drop of water run against gravity.[11] Other studies have shown that gradients of cross-sectional areas can also make capillary forces trigger the spontaneous motion of drops, bubbles and meniscii in conical wires and tubes and wedges.[12–15]

Here, we investigate the hitherto unreported case of soap films.

Sec. II describes the materials and procedures needed to record and analyze the temporal evolution of the position of a soap film moving spontaneously towards the narrow end of a funnel. In Sec. IV, where we model the flow using the assumptions and approximations discussed in Sec. III, we show that this spontaneous motion is driven by capillarity. Indeed, as discussed Sec. IV, capillary effects associated with the pressure drop across the curved soap film make it move from large to small funnel radius. This motion is resisted by viscous friction produced by the air flowing out of the geometry. Working within experimental conditions described in Sec. III, we use these simple physical arguments to determine the equation of motion of a film. Our results show that the duration of motion depends on five known geometric and physicochemical parameters and only one unknown quantity, the viscosity of air. Hence, this experiment allows the determination of air's viscosity from the measurements of the duration of motion of a curved soap film in a funnel. The resulting predictions compare well to systematic experiments in Sec. V. It is interesting to note that our experiment can be viewed as a capillary viscometer working for gases instead of liquids. A capillary viscometer is a common laboratory apparatus employed to determine the viscosity of a liquid by measuring the duration of motion of a liquid meniscus over a defined distance in a tube. Here, we measure the viscosity of a gas instead of that of a liquid, the soap film and the funnel playing the role of the liquid meniscus and tube, respectively. We finish with a few concluding remarks in Sec. VI.

II. EXPERIMENTS

Figure 1(a) shows the equipment needed to conduct experiments: soapy water, a funnel and some tubing. Before an experiment begins, the inner wall of the conical geometry, i.e., the funnel, is wetted with the soap solution used in our study (2 wt.% Palmolive Original (Colgate-Palmolive) and 98 wt.% deionized water). Herein, γ denotes the air-soap solution surface tension. The other relevant physicochemical parameters that are specified in Fig. 1(b) are the density and dynamic viscosity of air, ρ_a and η_a, respectively (see Fig. 1 and Fig. 2 which define the variables at play). Once the inner wall of the funnel is wetted, the wider end of the funnel of radius R is immersed into the solution a few millimeters below the free surface. It is convenient to move the funnel using either a manual laboratory scissor jack or a vertical linear stage (Aerotech ACT115DL) whose specifications can be found in a previous study.[16] However, the accuracy and precision of the measurements is unchanged if the funnel is moved by hand. We then remove the geometry quasistatically (the typical rate of motion is a few mm/s) with its axis of symmetry perpendicular to the liquid surface. When a circular ring of radius R is used

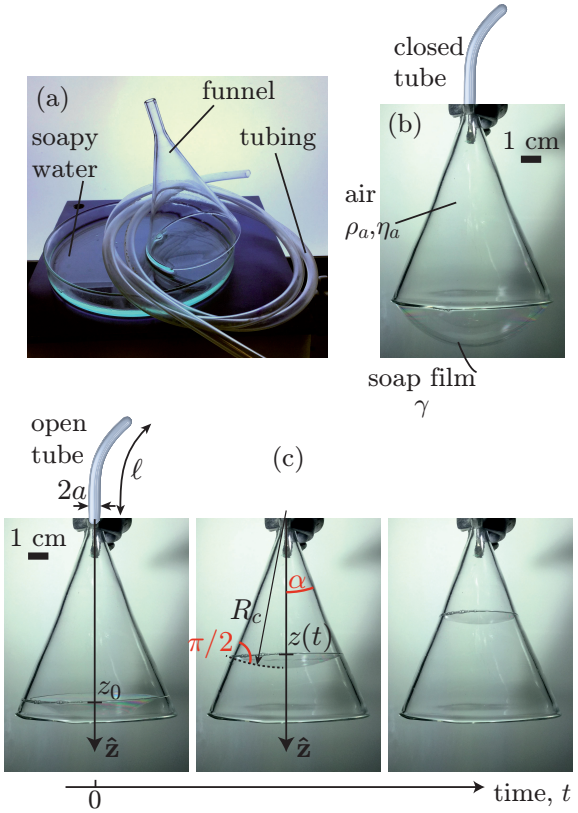

FIG. 1. (a) Photograph taken with the camera of a smartphone illustrating three elements needed to perform experiments to measure the viscosity of air: some tubing that can be connected to the narrow end of a funnel and soapy water. (b) A photograph of the preparation of an experiment: withdrawing the wider end of the funnel from a pool of the soapy water creates a curved soap film. (c) Series of photographs illustrating an experiment, i.e., the motion of a curved soap film in a funnel. In (b) and (c) some of the geometric and physicochemical parameters at play are defined. In these measurements, the geometrical parameters are: $a = 3.2$ mm, $\ell = 1$ m, and $\alpha = 22\ ^\circ$.

instead of a funnel, we have shown in a previous study that the process produces a catenoid made of a soap film between ring and free surface.[17] This surface of revolution becomes unstable above a critical height ($\approx 0.66R$) between geometry and free surface and collapses to leave a planar film on the ring and a surface bubble on the free surface.[17,18] Here, the process produces the same surface of revolution. However, in our experiments, the tube is closed before the critical height is reached so that the collapse of the catenoid yields the formation of a surface bubble and a curved soap film having the shape of a spherical cap on the wider end of the cone as shown in Fig. 1(b). If the tube is reopened, surface tension causes the curved film to self-propel towards the narrow end of the funnel (Fig. 1(c)). The propulsion of the film sets the air present in the funnel into motion.

During the preparation of our experiment, once the film with radius of curvature R_c is formed, the tube is reopened to allow the film to move towards the narrow

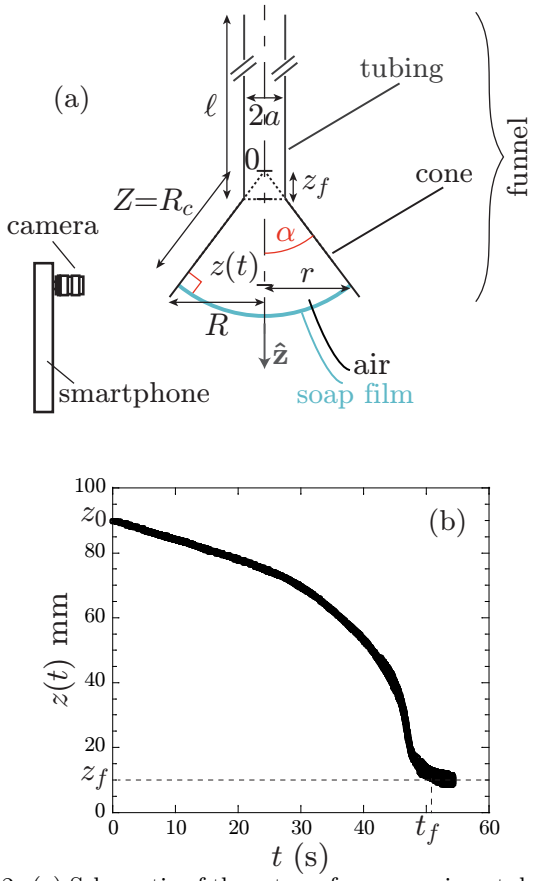

FIG. 2. (a) Schematic of the setup of our experiment defining the geometric and physicochemical parameters. (b) Temporal variations of the position of a film z obtained by processing a movie of an experiment using the method described in the text. As shown, the motion of the film begins at z_0 at $t = 0$ s and ends after a period of time t_f at $z_f = a/\tan\alpha$. This final experimental position is close to the expected value $a/\tan\alpha =$ 7.7 mm. In these measurements, the geometrical parameters are: $a = 3.2$ mm, $\ell = 1$ m, and $\alpha = 22.5$ °.

end of the funnel in the direction $-\hat{\mathbf{z}}$ [Fig. 1(c)]. It is stopped by closing the tube (length ℓ and radius a) when it reaches a desired initial position z_0 (see Fig. 1(c) and Fig. 2). We start the time ($t = 0$) when we reopen the tube and we record with a smartphone the temporal evolution of its position $z(t)$ (see Fig. 1(c) and Fig. 2) until it reaches a final one at $z_f = a/\tan\alpha$ (Fig. 2) where it stops; a is the radius of a tube and α is the half of its opening angle. In the experiment, we record the position z, but the analysis is performed in terms of $Z = z/\cos\alpha$; as shown in Fig. 2, Z is the distance between the apex of a cone and the point of contact of a film on a funnel wall which is also equal to the radius of curvature of the film, R_c. For the unidimensional motion of a soap film studied here, the free image analysis software ImageJ is used to find $Z(t)$.[19] Image processing consists of placing a line on an experimental movie along a soap films trajectory and creating a single image whose vertical axis is this line plotted for each frame of the movie as a function of time (horizontal axis of the image). Coordinates of each pixel of a binary version of the image can then be saved in a file that is imported with a free graphing software[20] to plot the position of a film as a function of time.

III. EXPERIMENTAL CONDITIONS, APPROXIMATIONS AND KEY VARIABLES

For these experiments and the interpretation of experimental results, we make five assumptions and/or approximations. As mentioned earlier, this study could teach undergraduate students that nontrivial measurements can be performed with common and inexpensive equipment. It could also teach them about the importance of approximations and assumptions in physics.

– First, we assume that air is incompressible and that a soap film is impermeable to this gas during the time of an experiment; hence, the mass and volume of air are conserved so that the volumetric flow rate, q, of air in a tube is given by the temporal variations of the volume of entrapped air in a cone.

– Second, in addition to the geometric and physicochemical quantities defined in Fig. 1 and Fig. 2, one could imagine that the thickness of a soap bubble film e or that of the film initially deposited on the inner wall of a geometry play a role (via gravity effects) in the experiment; films with different thicknesses are prepared using a method discussed in a previous work.[16] We use a spectrometer (Avantes AvaSpec-2048) to measure the thickness of a film. Experiments performed with the same geometry but different thicknesses of the deposited film (10–30 μm in our study) exhibit the same dynamics. Gravity effects (i.e., the estimate of the weight of a curved soap film $2\pi {Z_0}^2 e(1-\cos\alpha)\rho_\ell g$ with the gravitational acceleration g) should dominate over capillary action (i.e., the estimate of the total capillary force in the z-direction $4\pi Z_0 \gamma \sin\alpha$) when the thickness of a film e is larger than a threshold $e_c = 2\kappa^{-2} {Z_0}^{-1} \sin\alpha/(1-\cos\alpha)$ where $\kappa^{-1} = \sqrt{\gamma/(\rho_\ell g)}$ is the capillary length;[21] e_c is defined as that value of e for which the film weight equals the capillary force. Using typical values of the angle $\alpha = 22$ ° and initial position $Z_0 = 0.1$ m, the threshold thickness is larger than about 700 μm which is hundreds of times larger than the thickest films used in our study ($e = 1$–10 μm). Hence, we determine that gravity can be neglected when compared to surface tension in our study at the beginning of an experiment. To compare these two effects when a film moves over time, we assume that e remains constant between $t = 0$ and $t = t_f$. In order words, we assume that the liquid escapes through the meniscus on the wetted inner wall of the conical geometry as the film moves and its width decreases over time. Since the above expressions of the weight of a film and surface tension vary as Z^2 and Z, respectively, with Z decreasing over time, surface tension prevails for the whole dynamics and effects of gravity can be neglected over time. We would have liked to dismiss gravity as an important variable by showing that films moving in its di-

rection or against it give the same dynamics for the same experimental conditions. Unfortunately, results are altered when films move in the direction of gravity because some of the liquid move along the walls of the geometry and inside the tube.

– Third, we consider the idealized motion of soap films within a quasistatic limit that neglects the viscous drag acting on the meniscus linking a film to the wall of a cone. In other words, we consider the contact angle the film makes with the inner wall of a cone is $\pi/2$ at any time so that the radius of curvature of a soap film is $R_c = Z$ in our study (see Fig. 1(c) and Fig. 2 which define the variables at play). As shown by the illustrative example reported in Fig. 1(c), experimental observations made when the base of a film moves on the inner wall of a cone validate this assumption. Such an approach has been successfully employed to describe the motion of a single foam lamella flowing through a porous medium under applied pressure.[22,23] More recently, we have shown that this quasistatic approach can help rationalize one of the dynamics observed for shrinking surface bubbles.[6]

– Fourth, our modeling work considers that air is contained inside a complete cone instead of a truncated one attached to a tube. In other words, we model air flow with an excess volume of air $\pi a^3/(3\tan\alpha)$ corresponding to the cone of height $z_f = a/\tan\alpha$ and base with radius a whose contour is shown by the dashed lines in Fig. 2. Hence, the volume of air is $V = (2\pi/3)Z^3(1-\cos\alpha)$. This approximation seems reasonable since the excess volume is not a function of time and the model of the flow presented in Sec. IV uses the time derivative of the volume, i.e., the flow rate.

– Finally, we will show in Sec. IV that the air flow can be described by Poiseuille's equation that relates the pressure drop across the flow geometry, the flow rate, and the hydrodynamic resistance of the funnel. The studied geometry is a serial combination of a cone and a cylindrical tube. Hence its total hydrodynamic resistance is $R_h = R_{hc} + R_{ht}$ with R_{hc} and R_{ht} the resistances of the cone and the tube, respectively. As discussed more quantitatively in Sec. IV, the Reynolds number $\mathcal{R}_e$ associated with the air flow is small enough for this flow to be describe by the Stokes equation so that the resistance of a tube can be expressed in the well-known form $R_{ht} = 8\eta_a\ell/(\pi a^4)$.[24,25] The resistance of the conical part of the geometry is $R_{hc} = -\int_Z^{Z_f} 8\eta_a\cos\alpha/(\pi r(Z')^4)dZ' = 8\eta_a\cos\alpha\left({Z_f}^{-3} - Z^{-3}\right)/(3\pi(\sin\alpha)^4)$ with $r(Z) = Z\sin\alpha$ the radius of a film as defined in Fig. 2; this expression is valid for small angles α and and it is calculated within lubrication theory assuming a no-slip boundary condition.[26] When comparing the leading term of this resistance $[8\eta_a/(3\pi a^3\tan\alpha)]$ with that of a tube, we find that R_{hc} can be neglected when compared with R_{ht} when $\ell \gg a/(3\tan\alpha)$. In our experiments, for a typical funnel with $\alpha = 22\ ^\circ$, this condition becomes $\ell \gg 0.825a$ with $a = 1.5 - 5$ mm which is easily met experimentally when working with tubes having a length in the range $\ell = 0.01 - 10$ m. In this limit of long tubes, the hydrodynamic resistance of a cone is negligible compared to that of the tube, so we choose to work in this simplifying limit. In other words, $R_h \sim R_{ht}$ in what follows.

IV. MODEL OF THE FLOW

We consider that the motion of a film is driven by its curvature, i.e., by the Laplace pressure

$$\Delta p = \frac{4\gamma}{Z}, \tag{1}$$

which is the pressure difference across the curved film, from the air on one side of the film to the air on the other; γ is the air-liquid surface tension.[2] Indeed, surface tension, which an energy per unit surface area, can also be interpreted as a force per unit length acting on curved fluid-fluid interfaces such as the studied soap film moving in a conical flow geometry. In this case, surface tension produces an overpressure (well-known as the Laplace pressure) between the front of a film and the end of a tube at atmospheric pressure. The Laplace pressure is equal to the surface tension γ multiplied by (i) the sum of the two principal radii of curvature (here $1/(Z+e) + 1/Z \simeq 1/Z + 1/Z$) and (ii) a factor 2 that accounts for the two fluid-fluid interfaces forming a film; hence, equation (1) reads $\Delta p = 2\times 2\gamma/Z$.[2,27] Such a film then moves from high pressure (position of a film) to low pressure (end of a tube) regions.

The motion of a film is limited by the air flow that we consider to be one-dimensional and viscously dominated. Hence, the considered laminar air flow should satisfy the Poiseuille's equation that reads

$$\Delta p = R_h q, \tag{2}$$

where q is the air flow rate and Δp is the pressure difference between the position of a curved film and the end of a tubing which is at atmospheric pressure. For this experiment, as discussed in Sec. III, the flow can be considered to be laminar when the characteristic Reynolds number $\mathcal{R}_e$ is smaller than 2000.[24,28,29] In our experiment, this dimensionless quantity is obtained by comparing inertial $[\propto \rho_a v^2/(2a)]$ and viscous $[\propto \eta_a v/(2a)^2]$ body forces and reads $\mathcal{R}_e = 2a\rho_a v/\eta_a$;[29] v is the average velocity of the air flow and ρ_a is the air density, as illustrated in Fig.1(b) and Fig.2. The velocity v can be written $q/(\pi a^2)$ and, using Eqs. (1) and (2), q can be written $4\gamma/(ZR_h)$ so that $\mathcal{R}_e = 8\rho_a\gamma/(\pi aZR_h\eta_a)$. As we have shown in Sec. III that it is reasonable to approximate the total resistance R_h by that of the tube $R_{ht} = 8\eta_a\ell/(\pi a^4)$, the Reynolds number reads

$$\mathcal{R}_e = \frac{\gamma\rho_a}{\eta_a^2}\frac{a^3}{Z\ell}. \tag{3}$$

At the beginning of the motion of a film, $Z = Z_0$ is typically 0.1 m in our experiments. Also, for the soap solution used in our study, the air-liquid surface tension $\gamma = 25$ mN.m^{-1}; we measure γ with a simple method that involves recording a pendant drop of the soap solution with a smartphone.[1] Hence, using Eq.(3), the condition for laminar flow $\mathcal{R}_e < 2000$ is satisfied when $\ell > 1.7$ mm for the tube of smallest radius $a = 1.5$ mm and $\ell > 62.5$ mm for the largest tube's radius $a = 5$ mm.

Working within these limits and using the physical arguments described above, the combination of Eqs. (1) and (2) with the expression of the resistance of a tube gives

$$\frac{4\gamma}{Z} = \frac{8\eta_a \ell}{\pi a^4} q. \tag{4}$$

The flow rate is given by the temporal variation of the total volume of entrapped air,

$$q = -\frac{\mathrm{d}V}{\mathrm{d}t} = -2\pi Z^2 \frac{\mathrm{d}Z}{\mathrm{d}t}(1-\cos\alpha), \tag{5}$$

and substituting this expression into Eq. (4), we can write

$$\mathrm{d}t = -\frac{4\eta_a \ell(1-\cos\alpha)}{\gamma a^4} Z^3 \mathrm{d}Z. \tag{6}$$

The integration of Eq.(6) gives the following formula that describes the motion of a film

$$\left(\frac{Z(t)}{Z_0(t=0)}\right)^4 = 1 - \frac{\gamma a^4}{\eta_a \ell Z_0^4}\frac{1}{(1-\cos\alpha)} t = 1 - \frac{t}{t_f}, \tag{7}$$

with $t_f = \eta_a \ell {Z_0}^4 (1-\cos\alpha)/(\gamma a^4)$ the time at which air has escaped out of the cone and the film has reached its final position $z = z_f$. As discussed Appendix A, although we model the air flow with an initial volume of air larger than the experimental one (see Sec. III), the predicted time t_f should be very close to its experimental counterpart. Hence, knowing the geometric parameters of an experiment and the values of the liquid-air surface tension, measurements of t_f should allow one to determine the viscosity of air.

Similar physical arguments are used to determine the collapse time of a bubble in a deflating bubble experiment.[29] In such an experiment, a bubble placed on one end of a cylindrical tube deflates when the other end of the tube is opened and the pressured air in the bubble escapes through the tube.[29] The predicted collapse time can be used to determine the air-liquid surface tension of soap solutions.[30,31] However, these experiments with a non-moving bubble foot require a good image analysis program to obtain accurate data.[29] Here, as discussed at the end of Sec. II, analyzing an experiment only requires simple image processing performed with a free software.

V. EXPERIMENTAL RESULTS AND DISCUSSION

In this section we compare our model to experimental results. We investigate the motion of a film by varying either the opening angle of a cone 2α [Fig. 3(a)], or the length of a tube ℓ [Fig. 3(b)], or its its radius a [Fig. 3(c)], while maintaining other parameters fixed. As shown in these figures that report the temporal variations of the normalized position Z/Z_0 for these sets of experiments, the response qualitatively resembles that of Fig. 2(b) for all varied parameters: the normalized position is a monotonically decreasing function of time until the final position of a film is reached. When the experimental final time t_f is plotted as a function of α for given values of Z_0, ℓ and a, we find experiments are in qualitative agreement with predictions. Indeed, the inset of figure 3(a) shows that t_f increases with α and its predicted expression derived in Sec. IV varies as $(1-\cos\alpha)$ which for small enough α increases as α^2. Similar to these results, when the motion of a film is investigated for various ℓ and fixed α, Z_0 and a [see the inset of Fig. 3(b)], the results obtained for a wide range of tube length suggest t_f increases linearly with ℓ as predicted. Our experimental findings show much stronger dependence of the time t_f on the radius a [see the inset of Fig. 3(c) which reports these variations for fixed Z_0, ℓ and α] when compared to its variations with the length ℓ [inset of Fig. 3(b)]. Indeed, to increase the time at which a film stops by an order of magnitude, one can either increase the length of a tube by a factor of 50 or divide its radius by 2 [see Fig. 3(b) and Fig. 3(c)]. This result is also consistent with the predicted time t_f which varies both as ℓ and $1/a^4$.

To provide a more quantitative comparison between experiments and modeling, Figure 4 shows the variations with time of $(Z(t)/Z_0)^4$ for the experiments shown in Fig. 3. As expected by the form of Eq. (7), we find that the plotted quantity is a linearly decreasing function of time. Hence, the motion of a film is well-described by the quasistatic model with an air flow that satisfies Darcy's law and we can now compare measurements of the duration of motion with our prediction.

Figure 5 shows the evolution of the measured time t_f^{exp} as a function of the prediction $t_f^{th} = \eta_a \ell {Z_0}^4 (1-\cos\alpha)/(\gamma a^4)$ derived in Sec. IV. As shown in this figure, our simple model well describes the duration of motion since experiments mirror predictions for our whole set of data obtained with $\alpha = 15 - 30$ °, $Z_0 = 60 - 120$ mm, $a = 1.5 - 5$ mm and the length of a tube ℓ that is varied over more than three orders of magnitude $(0.01 - 12$ m). As shown in Fig. 6, these data can be used to determine the dynamic viscosity of air. All of our data points are within 20 % of the tabulated value of air viscosity ($\eta_a = 18.1$ μPa s) for the temperature at which data were taken (20 °C); more than 80 % of the data are within 10 % of this expected value (see Fig. 6). It is also important to note that the average value (17.75 μPa

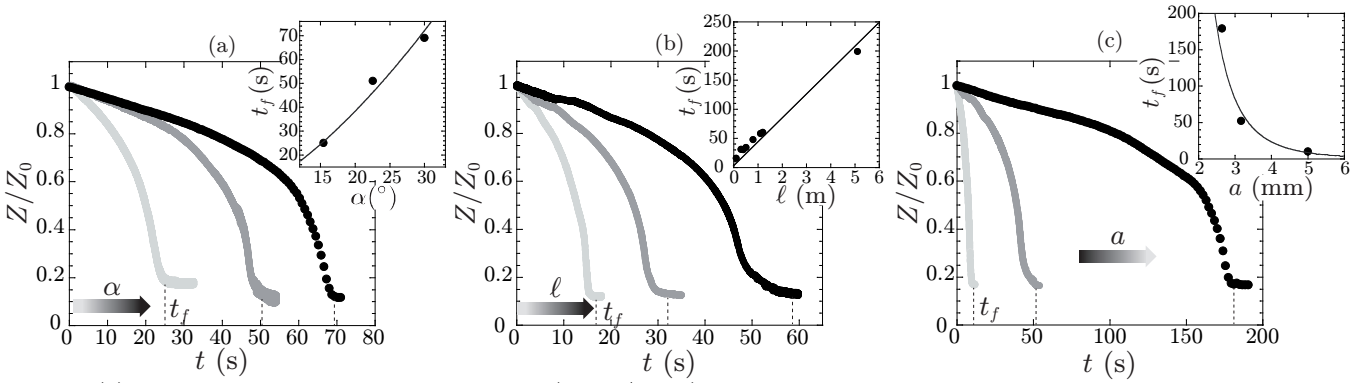

FIG. 3. (a) Temporal evolution of the position Z (i.e., $z/\cos\alpha$) of a film normalized by its initial position Z_0. The vertical dashed lines indicate the time t_f at which the motion of a film ends. Figure 3(a) shows the behavior with three values of α [(●) 15.5 °, (●) 22.5 °, (●) 30 °] for a tube of length and radius $\ell = 1$ m and $a = 3.2$ mm, and a fixed value of the position $Z_0 = 93 \pm 3$ mm. Figure 3(b) shows the variations of Z for three values of ℓ [(●) 110 mm, (●) 410 mm, (●) 1110 mm], an half-opening angle $\alpha = 21.25$ °, a radius of the tube $a = 3.2$ mm, and an initial position $Z_0 = 104 \pm 2$ mm. Figure 3(c) shows the behavior with three different radii a [(●) 2.65 mm, (●) 3.2 mm, (●) 5 mm] for an angle $\alpha = 21.75 \pm 0.5$ °, a tube of length $\ell = 1$ m and an initial position $Z_0 = 109 \pm 7$ mm.. Insets: Variations of the time t_f as a function of (a) α, (b) ℓ, and (c) a for the experiments shown the main plots in (a), (b), and (c); solid lines are guides for the eye.

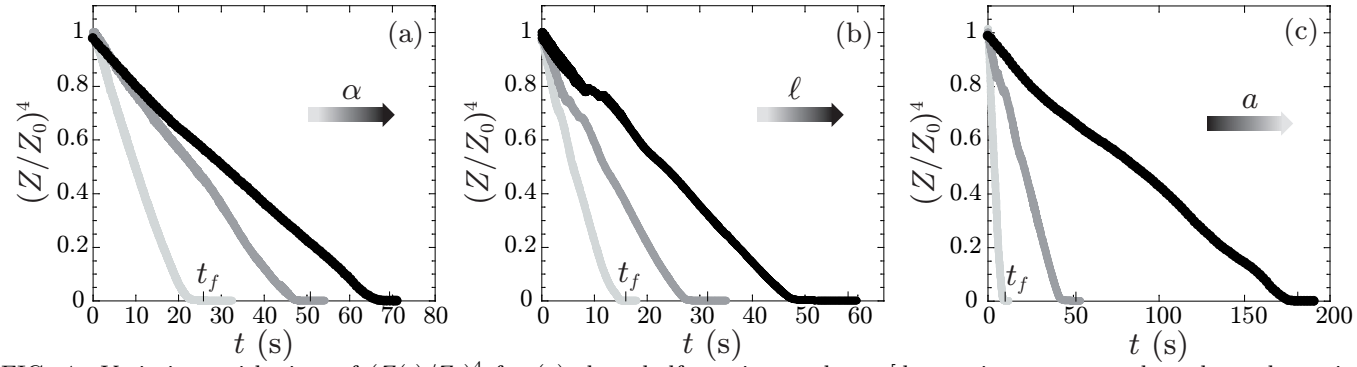

FIG. 4. Variations with time of $(Z(t)/Z_0)^4$ for (a) three half-opening angles α [data points correspond to those shown in Fig. 3(a)], (b) three values of ℓ [data points are those of Fig. 3(b)] and (c) three different radii a [data points are those reported in Fig. 3(c)]; other parameters are identical to those of Fig. 3. As predicted by our model, the plotted quantity in the three figures is a linearly decreasing function of time.

s) of the air viscosity deduced using our method is only 2.5 % smaller than the tabulated value which is remarkable considering the numerous approximations made to establish our model based on simple physical arguments. It is also worth mentioning that the standard deviation σ_η for the measurements shown in Fig. 6 is quite small, $\sigma_\eta = 1.54$ μPa s. Hence, our experiment offers a simple and inexpensive way to measure the dynamic viscosity of air.

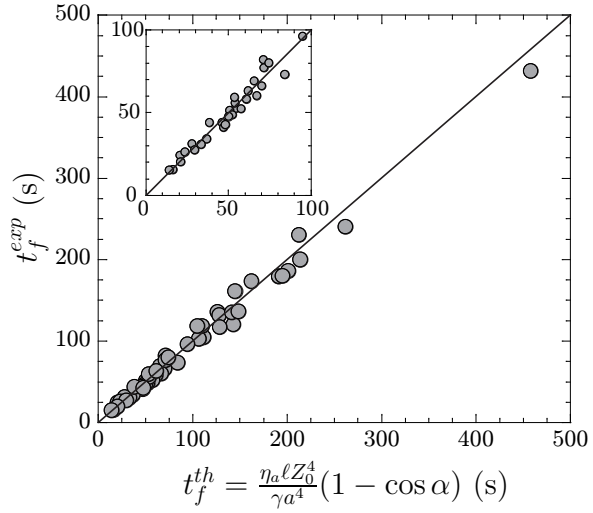

FIG. 5. Variations of the experimental time at which a film stops t_f^{exp} as a function of its theoretical counterpart t_f^{th} derived in the main text. Inset: magnification for times smaller than 100 s. The solid lines correspond to the best linear fit predicted by our model: $t_f^{exp} = t_f^{th}$. Each data point corresponds to a value of $\ell = 0.01 - 12$ m, $a = 1.5 - 5$ mm, $\alpha = 15 - 30$ °, and $Z_0 = 60 - 120$ mm.

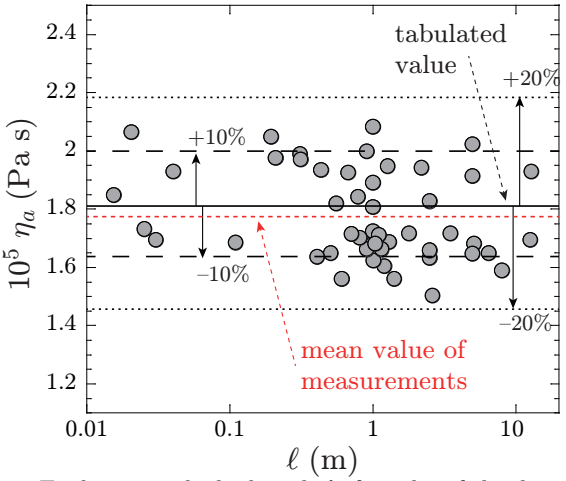

FIG. 6. Evolution with the length ℓ of a tube of the dynamic viscosity η_a of air determined from the measurements of the duration of motion of a film in a funnel as explained in the text. Parameters are identical to those of Fig. 5. The tabulated value of the viscosity of air (18.1 μPa s at 20 °C) is indicated by the black solid line. The average value of these measurements is 17.75 μPa s (red solid line).

VI. CONCLUSION

We have discussed a simple method to measure the viscosity of air that is directly applicable to the classroom. The experiments are easy to perform and analyze at low cost and the physics behind them can be taught to student in undergraduate physics courses. We have described five key assumptions and/or approximations so that students can also learn about the importance of reasonable approximations in physics research. In addition, using the setup described here, students will have the opportunity to observe a soap film propel itself against gravity. While beyond the scope of our paper, it is worthwhile mentioning this experiment can be extended to other situations that would require a more sophisticated experimental system. For instance, it could be used to determine the viscosity of other gases or that of air at different temperatures or relative humidity since a gas viscosity is a function of these physical quantities. Of course in that case, these measurements would demand not only a more refined setup but also the systematic determination of surface tension which decreases with increasing temperature (at a given relative humidity) or relative humidity (for a given temperature).

ACKNOWLEDGMENTS

We thank Franck Artzner for the rheometry that we used to determine the fluid viscosities, Benjamin Reichert and Arnaud Saint-Jalmes for the surface tension measurements and Lucie Pitois for flameworking the glass geometries used in this study.

Appendix A: Comparison between predicted and experimental times t_f

Here, we discuss the validity of our model which is based on several assumptions and approximations, including a slightly overestimated volume of air (see Sec. III). In what follows, t_f^{exp} and t_f^{th} denote experimental and theoretical times, respectively.

Using the physical arguments discussed in the main text, Eq. (7) describing the motion of a film is the solution of the following first-order ordinary differential equation:

$$Z^3 \mathrm{d}Z = -\frac{\gamma a^4}{4\eta_a \ell (1-\cos\alpha)} \mathrm{d}t. \tag{A1}$$

Using $t_f^{th} = \eta_a \ell {Z_0}^4 (1-\cos\alpha)/(\gamma a^4)$ the predicted period of time after which a film stops moving, Eq.(A1) can be written

$$\frac{\mathrm{d}t}{\mathrm{d}Z} = -4Z^3 \frac{t_f^{th}}{Z_0^4}.$$

Hence, the experimental time $t_f^{exp} = \int_0^{t_f} \mathrm{d}t$ reads

$$t_f^{exp} = \int_{Z_0}^{Z_f} \left(\frac{\mathrm{d}t}{\mathrm{d}Z}\right) \mathrm{d}Z = -t_f^{th} \frac{4}{Z_0^4} \int_{Z_0}^{Z_f} Z^3 \mathrm{d}Z$$

so that

$$t_f^{exp} = t_f^{th} \left[1 - \left(\frac{Z_f}{Z_0}\right)^4\right]. \tag{A2}$$

In our experiments, typical values of the initial (Z_0) and final (Z_f) positions of a film are 10^{-1} m and 10^{-2} m, respectively. Hence, the value of the term $(Z_f/Z_0)^4$ in Eq. (A2) is 10^{-4} so that t_f^{exp} should typically be 99.99% t_f^{th}. To conclude, the assumptions and approximations made to establish our model seem reasonable since the predicted time should compare very well with the measured one.

* pascal.panizza@univ-rennes1.fr
† laurent.courbin@univ-rennes1.fr

[1] N.-A. Goy, Z. Denis, M. Lavaud, A. Grolleau, N. Dufour, A. Deblais, and U. Delabre, "Surface tension measurements with a smartphone," Phys. Teach., **55**, 498-499 (2017).
[2] P. G. de Gennes, F. Brochard-Wyart, and D. Quéré, *Capillarity and Wetting Phenomena: Drops, Bubbles, Pearls, Waves* (Springer, New-York, 2004).
[3] L. Salkin, A. Schmit, P. Panizza, and L. Courbin, "Generating soap bubbles by blowing on soap films," Phys. Rev. Lett. **116**, 077801-1–5 (2016).
[4] R. M. Digilov and M. Reiner, "Weight-controlled capillary viscometer," Am. J. Phys., **73**(11), 1020-1022 (2005).
[5] Y. Shimokawa, Y. Matsuura, T. Hirano, and K. Sakai, "Gas viscosity measurement with diamagnetic-levitation viscometer based on electromagnetically spinning system," Rev. Sci. Instrum., **87**, 125105-1–4 (2016).
[6] M. Clerget, A. Delvert, L. Courbin, and P. Panizza, "Different scenarios of shrinking surface soap bubbles," Am. J. Phys. **89**(3), 244-252 (2021).
[7] For a short review on the pressure difference across a fluid interface (Laplace pressure), see for instance F. Behroozi and P. S. Behroozi, "Determination of surface tension from the measurement of internal pressure of mini soap bubbles," Am. J. Phys. **79**(11), 1089-1093 (2011).
[8] F. D. Dos Santos and T. Ondarçuhu, "Free-Running Droplets," Phys. Rev. Lett., **75**, 2972-5 (1995).
[9] Y. Sumino, N. Magome, T. Hamada, and K. Yoshikawa, "Self-Running Droplet: Emergence of Regular Motion from Nonequilibrium Noise," Phys. Rev. Lett., **94**, 068301-4 (2005).
[10] H. Linke, B. J. Alemán, L. D. Melling, M. J. Taormina, M. J. Francis, C. C. Dow-Hygelund, V. Narayanan, R. P. Taylor, and A. Stout, "Self-Propelled Leidenfrost Droplets," Phys. Rev. Lett., **96**, 154502-4 (2006).
[11] M. K. Chaudhury and G. M. Whitesides, "How to make water run uphill," Science, **256**, 1539-41 (1992).
[12] E. Lorenceau and D. Quéré, "Drops on a conical wire," J. Fluid Mech., **510**, 29-45 (2004).
[13] M. Reyssat, L. Courbin, E. Reyssat, and H. A. Stone, "Imbibition in geometries with axial variations," J. Fluid Mech., **615**, 335-344 (2008).
[14] P. Renvoisé, J. W. M. Bush, M. Prakash, and D. Quéré, "Drop propulsion in tapered tubes," EPL, **86**, 64003-5 (2009).
[15] E. Reyssat, "Drops and bubbles in wedges," J. Fluid Mech., **748**, 641-662 (2014).
[16] L. Salkin, A. Schmit, R. David, A. Delvert, E. Gicquel, P. Panizza, and L. Courbin, "Interfacial bubbles formed by plunging thin liquid films in a pool," Phys. Rev. Fluids **2**, 063604-1–10 (2017).
[17] L. Salkin, A. Schmit, P. Panizza, and L. Courbin, "Influence of boundary conditions on the existence and stability of minimal surfaces of revolution made of soap films," Am. J. Phys. **82**(9), 839-847 (2014).
[18] In our experiment, a surface bubble is a hemispherical bubble sitting on the liquid surface. The formation mechanisms of these bubbles and the variations of their size with the parameters of the experiment will be published elsewhere.
[19] <https://imagej.nih.gov/ij/>.
[20] <http://www.gnuplot.info/>.
[21] For a curved region of a fluid-fluid interface with typical length scale κ^{-1}, comparing an estimate of the Laplace pressure $\gamma\kappa$ to the hydrostatic pressure $\rho_\ell g\kappa^{-1}$ gives the capillary length $\kappa^{-1} = \sqrt{\gamma/(\rho_\ell g)}$. For length scales larger than κ^{-1}, gravity dominates. Otherwise, capillarity prevails over gravity.
[22] D. J. Ferguson and S. J. Cox, "The motion of a foam lamella traversing an idealised bi-conical pore with a rounded central region," Colloids Surf. A **438**, 56-62 (2013).
[23] W. R. Rossen, "Theory of mobilization pressure gradient of flowing foams in porous media," J. Colloid Interface Sci. **136**, 1-16 (1990).
[24] E. Guyon, J.-P. Hulin, L. Petit, and C. D. Mitescu, *Physical Hydrodynamics* (2nd ed., Oxford University Press, 2015).
[25] H. Bruus, *Theoretical Microfluidics* (Oxford University Press, 2008).
[26] S. Gravelle, L. Joly, F. Detcheverry, C. Ybert, C. Cottin-Bizonne, and L. Bocquet, "Optimizing water permeability through the hourglass shape of aquaporins," Proc. Natl. Acad. Sci. U.S.A. **110**(41), 16367–16372 (2013).
[27] L. Courbin and H. A. Stone, "Your wetting day," Phys. Today, **60**(2), 84-85 (2007).
[28] T. E. Faber, *Fluid Dynamics for Physicists* (Cambridge University Press, 1995).
[29] D. P. Jackson and S. Sleyman, "Analysis of a deflating soap bubble," Am. J. Phys., **78**, 990 (2010).
[30] L. Sibaiya, "Time of collapse of a soap bubble," Nature London, **149**, 527 (1942).
[31] Gören Rämme, "Surface tension from deflating a soap bubble," Phys. Educ. **32**, 191 (1997).